

PAPER • OPEN ACCESS

A spatial registration method for navigation system combining O-arm with spinal surgery robot

To cite this article: H Bai *et al* 2018 *J. Phys.: Conf. Ser.* **1016** 012006

View the [article online](#) for updates and enhancements.

You may also like

- [Behaviour of oxygen atoms near the surface of nanostructured Nb₂O₅](#)
U Cvelbar and M Mozeti
- [Intraoperative evaluation of device placement in spine surgery using known-component 3D–2D image registration](#)
A Uneri, T De Silva, J Goerres *et al.*
- [Investigation of O-atom kinetics in O₂, CO₂, H₂O and O₂/HMDSO low pressure radiofrequency pulsed plasmas by time-resolved optical emission spectroscopy](#)
A Bousquet, G Cartry and A Granier



ECS
The
Electrochemical
Society
Advancing solid state &
electrochemical science & technology

DISCOVER
how sustainability
intersects with
electrochemistry & solid
state science research

A spatial registration method for navigation system combining O-arm with spinal surgery robot

H Bai^{1,2}, G L Song¹ Y W Zhao¹ X Z Liu^{1,2} and Y X Jiang¹

¹Shenyang Institute of Automation, Chinese Academy of Sciences, China.

²Northeastern University, China.

Email: songgl@sia.cn

Abstract. The minimally invasive surgery in spinal surgery has become increasingly popular in recent years as it reduces the chances of complications during post-operation. However, the procedure of spinal surgery is complicated and the surgical vision of minimally invasive surgery is limited. In order to increase the quality of percutaneous pedicle screw placement, the O-arm that is a mobile intraoperative imaging system is used to assist surgery. The robot navigation system combined with O-arm is also increasing, with the extensive use of O-arm. One of the major problems in the surgical navigation system is to associate the patient space with the intra-operation image space. This study proposes a spatial registration method of spinal surgical robot navigation system, which uses the O-arm to scan a calibration phantom with metal calibration spheres. First, the metal artifacts were reduced in the CT slices and then the circles in the images based on the moments invariant could be identified. Further, the position of the calibration sphere in the image space was obtained. Moreover, the registration matrix is obtained based on the ICP algorithm. Finally, the position error is calculated to verify the feasibility and accuracy of the registration method.

1. Introduction

In the past two decades, minimally invasive spine surgery (MISS) has been increasingly applied and drawn much attention in the treatment of spinal disorders[1]. The development of image technology has led to a more significant development of minimally invasive spinal surgery. Not only can MISS minimize injury to paraspinal back muscles, connective tissues, and joints but it can also decrease the amount of bleeding, infection, hospital stay, and postoperative pain[2]. It decreases the incidence of complications and approach-related morbidity and mortality associated with conventional open surgery. The traditional open spine surgery has gradually been replaced with MISS. According to the reports[1], the number of MISS conducted in 2010 accounted for 1/6 of the total number of all spine surgeries in the United States and 1/3 in 2016, which is anticipated to be more than 1/2 in 2020.

Although MISS has the above advantages, it still faces to the following problems: (1) Surgeon's surgical vision is limited. (2) With the increasing number of surgery, the surgeon's intra-operative radiation exposure will accumulate. (3) The lack of surgical instrument's real-time position, reduces the safety of surgical procedures.

In order to solve the above problems, some scholars have proposed that the robot navigation technology could assist surgeons. A study assessed the feasibility and clinical value of robot assisted navigation drilling for pedicle screw placement and the results confirmed that robot assisted surgery could increase the quality of percutaneous pedicle screw placement[3]. The accuracy of guidance systems in screw insertion procedures is particularly notable in anatomically difficult cases, such as



scoliosis correction surgeries, with a reported 6-fold reduction in perforation rates and mean insertion angle errors compared with conventional methods[4]. In the meta-comparison of navigation-assisted versus conventional screw placement covering 28 clinical, 14 cadaveric, and 1 model-based study, Tian [5], reported a higher overall accuracy of screw position in navigation-assisted procedures.

The Rosa spine robot[6], which has been used clinically, combines robots and navigation systems to obtain the pose of surgical instruments and patients through two IR cameras. Under the assistance of intra-operative images, the surgical robot is guided to the surgical position and finally assists surgeons place pedicle screws. The navigation system of Rosa spine robot is through the optical imaging system to achieve spatial positioning and such systems are vulnerable to the effect of intra-operative objects' shelter, the surrounding light and metallic objects mirror reflection. What's more, the Renaissance guidance system[7], uses operating forceps or Hover-T to fix a miniature parallel robot on the patient's spine. The C-arm takes anterior–posterior and lateral intra-operative fluoroscopic images of the patient and transfers them to the workstation system for automatic image registration. But the specially designed jig with three marker holes need to be fixed to the patient's body, causing additional trauma to the patient.

In order to solve the above problems, this paper proposes a robotic navigation system based on O-arm. One of the major problems of this system is to registration of patient space and intra-operation image space. This study mainly introduces the registration method of the system.

2. Material and method

2.1. Material

This study designed a calibration phantom to assist spatial registration and error calculations. Taking the registration into account, the main criterion given for the phantom was the need to provide multiple surfaces for placement the calibration sphere[8]. The solution for this criterion was to design a 70mm × 70mm × 80mm cube calibration phantom. The four faces of which are accurately placed with calibration holes, each with 16 calibration holes on each plane to provide sufficient test volume. Figure 1 illustrates the used calibration phantom. The calibration holes were machined 15mm apart, and the position error for the distance horizontally and vertically was within ± 0.02 mm. The diameter and depth of the calibration hole is 2.5 mm, which ensures that the calibration sphere is exactly filled in the hole.

The use of O-arm has been increasing in recent years, because the medical staff can leave the operating theatre to decrease their exposure to radiation, during an O-arm 3D image acquisition[9]. The O-arm is a mobile intra-operative computed tomography imaging system optimized for bony structures in spinal and orthopedic surgery [10]. Pixel size is 0.424×0.424 mm within a slice thickness of 0.625 mm. Figure 2 illustrates the calibration phantom and the spinal phantom with the O-arm.

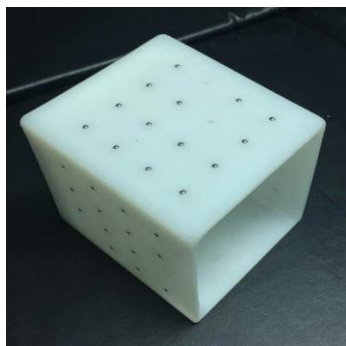


Figure 1. The present calibration phantom.



Figure 2. The two phantom with O-arm.

2.2. Methods

Connecting the calibration phantom and the Stäubli robot through the connecting rod. Figure 3 illustrates the way of connection between the calibration phantom and robot. The position of the calibration sphere in the patient space is obtained by the kinematics of the robot. Scanning the calibration phantom and the spinal phantom together by the O-arm to obtain CT slices containing both phantoms. The robot and the connecting rod are kept at a certain distance from the scanning area to prevent serious metal artifacts in the CT slices, during the O-arm scanning.

The material of the calibration sphere placed in the phantom is metal. The gray-scale value of the calibration sphere is very different from the gray-scale value of the calibration phantom in the CT slices. Therefore, it is easy to identify the calibration sphere in the slices. Although the O-arm from the multi-angle fluorescence projection to the CT slice is very fast, there are metal artifacts around calibration spheres in the CT slices, due to beam hardening. Figure 4 illustrates one of the CT slices containing metal artifacts. Metal artifacts result in dimensional distortion of the slices of the calibration sphere, which require to reduce to improve the accuracy of image feature extraction.



Figure 3. Connection between the phantom and robot.

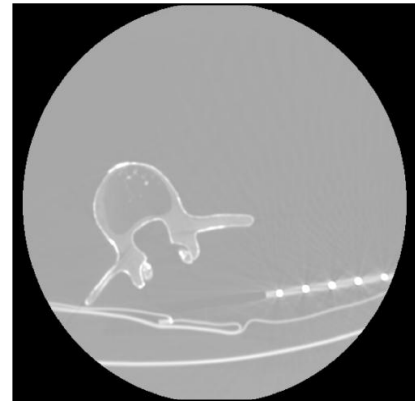


Figure 4. CT slice with metal artifacts.

Metal artifact reduction.

Most metal artifact reduction (MAR) researches focused on the development of methods which use raw CT scan data. But in most applications, the raw data is not available and researchers can only infer the true results from the containing artifacts filtered back projection (FBP) images. In order to solve this problem, Naranjo[11], made the FBP image be converted to the polar coordinate system, before the image processing. And the streaking artifacts are converted into vertical rays, which can be easily removable using a morphological filter. This method was used for metal artifact reduction because of the radial artifacts that occur around the calibration sphere in the CT slices, resulting in its shape being not a standard circle.

The purpose is to preserve the original structure of the initial image as much as possible while reducing artifacts. The result of closing–opening average filter, as in equation (1) is the average of the results of the closing and opening operators. The maximum gray-scale value changes the smallest and the noise gray-scale value changes the maximally. That is the best reduction results.

$$\text{COA}_\lambda = \frac{\gamma_{B_\lambda}(f) + \varphi_{B_\lambda}(f)}{2} \quad (1)$$

The results of the morphological filters are associated not only with the type of filter but also with the correct selection of the shape and size of structuring element (SE). To overcome this problem a distance adaptive size of the SE is used. Let $\lambda = 2 \square 20$. Using the center point of the artifact as the origin of the coordinate transformation. The transformation into polar coordinates is defined by the following equation (2):

$$\rho = \sqrt{(x - x_c)^2 + (y - y_c)^2}, \quad 0 \leq \rho \leq \rho_{\max}$$

$$\theta = \arctan\left(\frac{y - y_c}{x - x_c}\right), \quad 0 \leq \theta \leq 2\pi \quad (2)$$

Defining (x_c, y_c) as the origin of the streaking rays, that is, taking the streaking source as the focus of the transformation.

Using line detection and Hough transform to extract striped artifacts[12]. Figure 5 is a flow chart for obtaining the center coordinates of the metal object.



Figure5. The flow chart for obtaining the metal center coordinates.

The basic steps are as follows:

(1) Extracting stripe artifacts by line detection and Hough transform to find the center coordinates of metal objects.

(2) Converting the initial image from the Cartesian coordinate system to the polar coordinate system.

(3) In the polar coordinate system using closing–opening filter to remove artifacts.

(4) The filtered image is converted from the polar coordinate system to the Cartesian coordinate system to obtain $I_{filtered}$.

(5) The initial image is processed by threshold to get I_{msk} .

(6) The final image is obtained by combining the initial image with the filtered image, as in equation (3).

$$I_{output} = I_{original} \times I_{filtered} \times (1 - I_{msk}) \quad (3)$$

Circle recognition. In order to improve the speed of image feature recognition and shorten the operation time, the moment invariants of the images were used to represent the shape features of the sectional circles of the metal spheres in the CT slices. Moment invariants are very useful tools for pattern recognition. They were firstly derived by Hu in 1963 which were frequently used as features for shape recognition [13] and Hu's invariants are usable based on region. Then Chen [14] has proposed improved moment invariants based on boundary in 1993. Both the above-mentioned features are not valuable based on both regions and boundaries simultaneously. So we use the united moment invariants derived by Sun[15] which can be applied based on both region and boundary. Sun derived the following moment invariants, as in equation (4):

$$\begin{cases} \theta_1 = \sqrt{\phi_2} / \phi_1 & \theta_2 = \phi_6 / \phi_1 \phi_4 \\ \theta_3 = \sqrt{\phi_5} / \phi_4 & \theta_4 = \phi_5 / \phi_3 \phi_4 \\ \theta_5 = \phi_1 \phi_6 / \phi_2 \phi_3 & \theta_6 = (\phi_1 + \sqrt{\phi_2}) \phi_3 / \phi_6 \\ \theta_7 = \phi_1 \phi_5 / \phi_3 \phi_6 & \theta_8 = (\phi_3 + \phi_4) / \sqrt{\phi_5} \end{cases} \quad (4)$$

Where ϕ_i are Hu's moment invariants.

Sphere center calculation. Through identifying the position of the circle in the CT slices by the above eight formulas, but the problem is lacking the depth information about the center of the sphere. We need to obtain the radius of the circle and the radius of the sphere to compute the depth information. It is known that any section of the sphere must be circular, and the circle of the center of

the circle and the core of the connection will be perpendicular to the cross section. Through the experiment, we found that the position of the center of the same sphere was almost constant. So it was possible to use the Pythagorean theorem to find the distance from the cross section to the center of the sphere. Because the direction of the center of the sphere is uncertain, two distances were obtained with depth information for each section. The trend of the radius changing can exclude the false distance and keep the true distance. The center of the sphere is represented by the average of the depth information about a sphere in the intra-operation image space.

Spatial registration algorithm. ICP algorithm has the advantages of fast convergence speed. The spatial transformation parameter of point set is the spatial mapping parameter of image. The registration algorithm consists of two steps: preregistration and precise registration.

A good initial value is important to the iterative algorithm, because it can prevent the optimal solution from falling into the local minimum solution and reduce the time consumption of the registration algorithm. The initial registration is used to provide an iteration initial value near the global optimal solution. Finding the pre-selected four non-coplanar mark points, through these four points to complete the pre-registration. The four marked points in patient space and intra-operation image space form two matrices P_R^M and P_i^M , respectively, as shown in equation (5) and (6).

$$P_R^M = \begin{bmatrix} x_R^1 & x_R^2 & x_R^3 & x_R^4 \\ y_R^1 & y_R^2 & y_R^3 & y_R^4 \\ z_R^1 & z_R^2 & z_R^3 & z_R^4 \\ 1 & 1 & 1 & 1 \end{bmatrix} \quad (5)$$

$$P_i^M = \begin{bmatrix} x_i^1 & x_i^2 & x_i^3 & x_i^4 \\ y_i^1 & y_i^2 & y_i^3 & y_i^4 \\ z_i^1 & z_i^2 & z_i^3 & z_i^4 \\ 1 & 1 & 1 & 1 \end{bmatrix} \quad (6)$$

The pre-registration matrix ${}^i T_r^1$ is shown in equation (7).

$${}^i T_r^1 = P_i^M (P_R^M)^{-1} \quad (7)$$

After the pre-registration matrix is obtained, the point cloud in patient space P_r can be converted to P_r' by pre-registration matrix ${}^i T_r^1$, as shown in equation (8). Then the pre-registration is completed.

$$P_r' = {}^i T_r^1 P_r \quad (8)$$

After pre-registration, the relationship between the patient space and the intra-operation image space can be calculated. ICP registration algorithm is used to accomplish precise registration, which was first proposed by Besl and Mckay[16], the essence of which is that based on least squares registration. The rotation matrix R and the position vector P are updated until equation (9) is satisfied. Finally, the registration matrix ${}^i T_r^2$ was obtained.

$$f(R, T) = \sum_{k=1}^n \|P_i^{k'} - (R P_r^k + T)\|^2 = \min \quad (9)$$

3. Results

After obtaining the CT slices, the DICOM format is converted to BMP format, which will increase the speed of the next processing. The BMP format image is Gaussian filter, Canny edge detection and contour extraction, calculate the moment invariants of each contour. When the condition is met, the contour ellipse is fitted again, and Figure 6 shows the result of the recognition based on the moment invariants, where the identified ellipse is highlighted in red. The elliptical maximum inscribed circle is defined as the sectional circle of the calibration sphere, so the circle radius is elliptical short axis, and the center of the circle is the center of the ellipse.

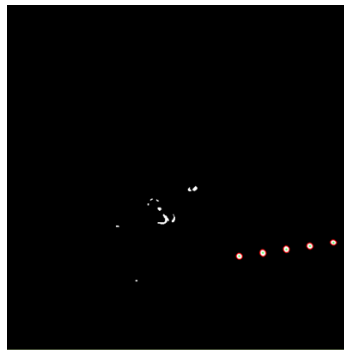


Figure 6. The red oval for the fitting results.

By moving the robot, scanning again and the second set of data was obtained to calculate the error. The center position (X_r^e, Y_r^e, Z_r^e) in the patient space is multiplied by the registration matrix ${}^i T_r^2$. The calculated results are compared with the centroid position (X_i^e, Y_i^e, Z_i^e) in the image space. The error analysis is based on the position error between the calculated sphere center coordinates and the sphere center coordinates obtained by the robot kinematics, as shown in equation (10). Figure 7 illustrates the histogram of the position error.

$$\text{Error} = |(\text{calculated value}) - (\text{true value})| \quad (10)$$

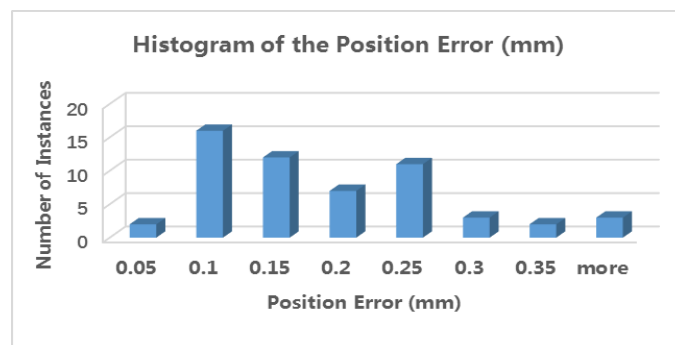


Figure 7. The histogram of the position error.

4. Conclusions

In this study, metal artifact reduction, feature recognition based on moment invariants and spatial registration method based on ICP were used to calculate the position of the same group of spheres in different spaces, and the registration of intra-operation image space and patient space was realized. In order to solve the intra-operative combination of the O-arm and the robot navigation problem, without increasing the patient's additional trauma, the idea of mechanical positioning navigation is proposed. A new way of consideration is provided for the surgery robot navigation technology.

But there are still the following questions:

First, the experimental process need to maintain the relative fixation of the vertebral body, spinal movement or other deformation will lead to a decline in navigation accuracy.

Second, because the validity of the algorithm is affected by the reconstructed FBP image quality and the effect of the morphological filter, the image effect of the artifacts that are not serious is not significant, and the adaptability of the morphological filter will be strengthened.

It is necessary to research the above issues in later studies.

References

- [1] Huang T J, Kim K T, Nakamura H, Yeung A T and Zeng J 2017 *Biomed Research International* **2017**(5) pp 1-4
- [2] Kim J S, Härtl R and Mayer H M 2016 *Biomed Research International* **2016** pp 5048659

- [3] Hongwei W, Yue Z, Jun L, Jianda H and Liangbi X 2015 *Indian Journal of Orthopaedics* **49**(4) pp 452-457
- [4] Keric N, Doenitz C, Haj A, Rachwalczewicz I, Renovanz M, Dma W, et al. 2017 *Neurosurgical Focus* **42**(5) pp E11
- [5] Tian N F, Huang Q S, Zhou P, Zhou Y, Wu R K, Lou Y, et al. 2011 *European Spine Journal* **20**(6) pp 846-859
- [6] Lefranc M and Peltier J 2015 *Journal of Robotic Surgery* **9**(4) pp 331-338
- [7] Sukovich W, Brinkdanan S and Hardenbrook M 2006 *International Journal of Medical Robotics & Computer Assisted Surgery* **2**(2) pp 114-22
- [8] Koivukangas T and Katisko J P A 2010 *5th Cairo International Biomedical Engineering Conference* (Cairo, Egypt) pp 57-60
- [9] Pitteloud N, Gamulin A, Barea C, Damet J, Racloz G and Sans-Merce M 2016 *European Spine Journal* **26**(3) pp 1-7
- [10] Koivukangas T, Katisko J P and Koivukangas J P 2011 *Conf Proc IEEE Eng Med Biol Soc* **2011**(4) pp 2148-2151
- [11] Naranjo V, Lloréns R, Alcañiz M and López-Mir F 2011 *Computer Methods & Programs in Biomedicine* **102**(1) pp 64-74
- [12] Naranjo V, Llorens R, Paniagua P and Albalat S 2009 *International Work-Conference on the Interplay Between Natural and Artificial Computation* (Springer, Berlin, Heidelberg) pp 11-19
- [13] Hu M K 1962 *IRE transactions on information theory* **8**(2) pp 179-187
- [14] Chen C C 1993 *Pattern Recognition* **26**(5) pp 683-686
- [15] Sun Y, Liu W and Wang Y 2003 *IEEE International Conference on Robotics, Intelligent Systems and Signal Processing, 2003. Proceedings* (Changsha, Hunan, China) 1 pp 88-93
- [16] Besl P J and McKay N D 1992 *IEEE Transactions on pattern analysis and machine intelligence* **14**(2) pp 239-256

Acknowledgments

This work was supported in part by National Natural Science Foundation of China (Grant No. 61333019 and 61703394).